Engineering 42 (2024) 26–38

Contents lists available at ScienceDirect

Engineering

journal homepage: www.elsevier.com/locate/eng

Research
Precision Nutrition and Health—Article

# Skin Rejuvenation in Aged Mice by Fecal Microbiota Transplantation from Young Mice Feces

Shoujuan Yu [a,#], Ziyang Li [a,#], Xiaoxu Zhang [a], Qi Zhang [b], Liwei Zhang [a], Liang Zhao [c], Ping Liu [c], Jie Guo [a], Juan Chen [a], Chengying Zhang [d], Xinjuan Liu [e], Mengyang Yu [d], Dekui Jin [d], Xiaofeng Wang [f], Guang Li [e], Yan Cao [d], Fazheng Ren [b,*], Ran Wang [a,*]

[a] Key Laboratory of Functional Dairy, Co-Constructed by Ministry of Education and Beijing Government, Department of Nutrition and Health, China Agricultural University, Beijing 100193, China
[b] Advanced Innovation Center for Food Nutrition and Human Health, Department of Nutrition and Health, China Agricultural University, Beijing 100193, China
[c] Research Center for Probiotics, China Agricultural University, Beijing 100083, China
[d] Department of General Practice, The Third Centers of Chinese PLA General Hospital, Beijing 100039, China
[e] Department of Gastroenterology, Beijing Chaoyang Hospital, Capital Medical University, Beijing 100020, China
[f] Department of Gastroenterology, The Third Centers of Chinese PLA General Hospital, Beijing 100039, China

ARTICLE INFO

*Article history:*
Received 24 March 2024
Revised 24 July 2024
Accepted 9 August 2024
Available online 26 August 2024

*Keywords:*
Skin aging
FMT
Tryptophan
Indole-3-lactic acid
AhR
Epidermal differentiation

ABSTRACT

Skin aging is an increasingly prominent topic in the context of healthy aging. During the aging process, the skin's barrier function diminishes, its water content decreases, wrinkles begin to form, and changes occur in the gut microbiota composition. However, the relationship between gut microbiota and skin aging remains unclear. In this study, we explored skin rejuvenation in aged mice through fecal microbiota transplantation (FMT) using feces from young mice. The results demonstrated enhanced water retention, thickened stratum corneum, increased collagen content, and improved epithelial cell differentiation in aged mice following FMT. Notably, FMT particularly increased the abundance of *Lactobacillus* and *Lactococcus* in aged mice, which were nearly undetectable in untreated aged mice. Non-targeted and targeted metabolomics analyses indicated that FMT significantly elevated levels of tryptophan (Trp) and its microbiota metabolites (e.g., indole-3-lactic acid (ILA)) in the feces and serum of aged mice. Both Trp and ILA appeared to rejuvenate aged skin by activating the aryl hydrocarbon receptor (AhR) to promote epidermal cell differentiation. In conclusion, FMT from young mice rejuvenated aged skin via Trp-metabolizing bacteria (*Lactobacillus* and *Lactococcus*) and Trp-derived metabolites, suggesting that interventions targeting Trp metabolites may effectively improve skin aging.



## 1. Introduction

The skin has the largest surface area in the body, is in direct contact with the external environment, and plays a crucial role in protecting and regulating bodily homeostasis [1–3]. Premature skin aging is associated with undesirable aesthetic changes and impaired skin function, such as decreased moisture content, increased transepidermal water loss, and reduced collagen content, which collectively leads to diminished skin thickness and barrier function [4]. During aging, more pronounced skin changes occur, including the development of wrinkles and pigmentation. The primary cause of skin aging is cellular senescence, during which cell properties and composition change with age, adversely affecting the structural scaffolds and ecological niches for epidermal stem cells [5–7]. Moreover, skin cell proliferation and differentiation decrease, accompanied by a gradual decline in skin cell regeneration, ultimately leading to skin aging and senescence [8–11].

Skin aging has garnered considerable research attention, prompting a surge in efforts to identify ways to reverse the process, particularly in the fields of medical aesthetics and anti-aging. Currently, skin aging can be delayed using topical and oral supplements [12]. Some topical anti-aging skincare products, such as hyaluronic acid and collagen, are applied to the skin's surface

* Corresponding authors.
*E-mail addresses:* renfazheng@cau.edu.cn (F. Ren), wangran@cau.edu.cn (R. Wang).
# These authors contributed equally to this work.

https://doi.org/10.1016/j.eng.2024.08.005

and may temporarily improve water retention, but they do not provide long-term benefits for skin function [13]. Oral supplements offer a systemic approach to enhancing skin aging from within. Substances reported to improve skin aging include vitamins C and E, probiotics, and others [14,15]. Vitamins C and E slow down skin aging by scavenging free radicals from the body. Oral probiotic supplements, such as *Lactobacillus casei*, may improve skin inflammation and acne by accelerating skin barrier restoration [16–18]. *Bifidobacterium longum* and its tryptophan (Trp) metabolite indole-3-carbaldehyde ameliorate atopic dermatitis inflammation by activating the aryl hydrocarbon receptor (AhR), which promotes epidermal differentiation [19].

Since gut microbiota composition is highly complex, with many bacteria that cannot be cultured, it is challenging to maximize bacterial effects through the oral intake of single probiotic products. Therefore, fecal microbiota transplantation (FMT) has been widely used to treat various dysbiosis-associated diseases [20,21]. FMT involves a comprehensive alteration of the gut flora, where the donor flora has established a stable relationship in its intestinal tract, making it one of the most direct methods to introduce a wide range of probiotics and rapidly modify the intestinal microbiota. FMT has been reported as a treatment for skin diseases, gastrointestinal disorders, metabolic syndrome, and cancer [22]. For instance, FMT has been shown to overcome resistance to anti-programmed cell death protein 1 therapy in skin cancer patients [23]. Additionally, FMT has suppressed atopic dermatitis-induced allergic reactions by restoring gut microbiota and immune balance [24]. However, the effects of FMT on aging skin require further investigation.

Studies have also reported that gut dysbiosis promotes organ aging (e.g., skin) primarily through inflammation and damage to the skin barrier [24,25]. FMT co-habitation studies are commonly used to address gut dysbiosis [26–28]. Therefore, it may be possible to delay skin aging by modulating the host microbiota. In this study, we altered the gut microbiota in aged mice via FMT from young mice and identified beneficial bacteria and associated metabolites that improved skin aging.

## 2. Methods

### 2.1. FMT animal studies

Young (2 months old, $n$ = 6) and aged C57BL/6 J male mice (24 months old, $n$ = 12, divided into two groups: Old and Old-Y) were obtained from PHENOTEK Biotechnology Co., Ltd. (China). Mice were housed in a laboratory animal facility at China Agricultural University, acclimatized for one week, and fed a standard diet. The facility was maintained at 22–25 °C with 60% relative humidity and a 12 h/12 h light/dark cycle. Animal studies were approved by the Animal Experimentation Ethics Committee at China Agricultural University (approval code: AW82303202-5-1).

### 2.2. Inoculum preparation for FMT

As FMT donor samples, feces from young mice were collected under strict anaerobic conditions. Samples (120 mg) were homogenized in ice-cold phosphate-buffered saline (PBS) (1 mL), centrifuged at 800*g* for 10 min at 4 °C, and the supernatants were transferred to tubes and stored at −80 °C [29].

### 2.3. The FMT protocol

Mice were randomly divided into three groups ($n$ = 6 per group): ① Young mice gavaged with PBS, ② Old mice gavaged with PBS, and ③ Old-Y mice gavaged with fecal supernatant samples from young mice. Before FMT, Old-Y mice were gavaged with a cocktail of broad-spectrum antibiotics, including ampicillin (1 $g{\cdot}L^{-1}$), vancomycin (0.5 $g{\cdot}L^{-1}$), neomycin (1 $g{\cdot}L^{-1}$), and metronidazole (1 $g{\cdot}L^{-1}$) for two weeks. Old-Y mice then received a daily 200 μL fecal mixture by gavage for one month [29].

### 2.4. Hematoxylin and Eosin (HE) staining

Skin samples were placed in neutral fixatives, dehydrated in alcohol, and embedded in paraffin. HE staining procedures were performed according to kit instructions (G1120, Solarbio, China). ImageJ (version 4.0.2, Scion Corp., USA) was used to measure skin and epidermis thickness. Epidermis thickness was quantified by measuring the distance from the stratum corneum to the stratum basal.

### 2.5. Masson staining

Masson staining sections were 5 μm thick, and staining was performed according to the kit instructions (G1340, Solarbio). ImageJ was used to measure collagen volume ratios.

### 2.6. Immunofluorescence (IF) staining

Dorsal skin samples were taken, fixed in neutral fixative for 24 h, and 5 μm thick sections were used for IF staining. Samples were incubated with anti-cytokeratin 10 (ab76318, Abcam (UK), 1:200), anti-desmoglein 1 (ab124798, Abcam, 1:100), and anti-loricrin (ab85679, Abcam, 1:100) primary antibodies, followed by fluorescent secondary antibodies. Images were acquired using a Leica DM1000 microscope and Leica Microsystems imaging software (Leica, Germany) was used to acquire images.

### 2.7. Skin properties

Skin property tests were conducted based on Kim et al. [30] with some modifications. Mice were dorsally shaved the day before skin characterization. A VapoMeter (Delfin, Italy) measuring probe was placed on the bare dorsal skin surface, and trans-epidermal water loss (TEWL) values were recorded after readings had stabilized.

### 2.8. Western blotting

A radioimmunoprecipitation solution was used to extract proteins from skin samples. Target proteins were separated using sodium dodecyl sulfate-polyacrylamide gels, transferred to polyvinylidene fluoride membranes, and incubated with the following primary antibodies: collagen I (CST (USA), 72026, 1:1000), collagen III (Santa Cruz Biotechnology (USA), sc-271249, 1:1000), β-actin polyclonal (Proteintech, 20536-1-AP, 1:1000), ZO1 (Proteintech (USA), 21773-1-AP, 1:1000), occludin (Servicebio (China), GB111401, 1:1000), claudin-1 (Proteintech, 28674-1-AP, 1:1000), AhR (Proteintech, 28727-1-AP, 1:1000), and CYP1A1 (Proteintech, 13241-1-AP, 1:1000). The membranes were then incubated with a horseradish peroxidase-conjugated secondary antibody for 60 min. A chemiluminescence reagent was used to detect protein signals.

### 2.9. 16S ribosomal RNA (rRNA) sequencing

Fecal samples were collected from mice between 9 and 10 a.m. at baseline and after four weeks of intragastric administration, and were immediately frozen at −80 °C. Fecal DNA was extracted using a DNA extraction kit. The V3–V4 region of bacterial 16S rRNA was amplified using 341F (5′-CCTACGGGNGGCWGCAG-3′) and 806R

(5′-GGACTACHVGGGTATCTAAT-3′) barcoded primers. Data processing and analyses were performed on the Majorbio cloud platform (China). To obtain high-quality clean reads, raw reads were further filtered according to the following rules using FASTP (version 0.18.0): reads containing more than 10% unknown nucleotides and less than 50% of bases with quality > 20 were removed. Paired-end clean reads were merged as raw tags using FLASH (version 1.2.11) with a minimum overlap of 10 base pairs (bp) and mismatch error rates of 2%. Operational taxonomic units (OTUs) with a 97% similarity cutoff were clustered using UPARSE version 7.1, and chimeric sequences were identified and removed. The lowest taxonomic annotation for an OTU was defined as having a consensus assignment score of $\geq$ 70. The significance of α-diversity was assessed by the Kruskal–Wallis test. A $p$ value < 0.05 was considered statistically significant.

### 2.10. Untargeted fecal metabolomics using a Gas Chromatography-Time of Flight-Mass Spectrometer (GC-TOF-MS)

Fecal samples (50 mg), including the internal standard (alditol at 0.5 mg·mL$^{-1}$), were extracted in methanol/acetonitrile (ACN)/$dH_2O$ (v:v:v = 2:2:1) and processed with a 35 Hz grinding instrument for 4 min. Samples were then mixed and centrifuged at 12 000$g$ at 4 °C for 15 min to obtain 200 μL supernatants. Quality control (QC) samples consisted of a homogeneous mixture of all samples. After evaporation in a vacuum concentrator, methoxyamine hydrochloride (20 mg·mL$^{-1}$ in pyridine) and BSTFA reagent (1% TMCS) were used to derivatize the supernatants. A 5 μL aliquot of FAMEs (in chloroform) was added to the QC sample.

GC-TOF-MS (Agilent 7890) was used to analyze the samples [31] on a DB-5MS capillary column, with a 1 μL aliquot injected in splitless mode. The carrier gas was helium (flow rate = 3 mL·min$^{-1}$ at the inlet and 1 mL·min$^{-1}$ through the column). The initial temperature was 50 °C, which increased to 310 °C. The injection and transfer line temperatures were 280 °C, and the ion source temperature was 250 °C. The energy was −70 eV in electron collision mode. Mass spectral data were acquired in full scan mode over the 50–500 mass-to-charge ratio ($m/z$) range, with a solvent delay of 6.4 min at 12.5 spectral bands·s$^{-1}$.

Raw data analysis, including peak extraction, baseline adjustment, deconvolution, alignment, and integration, was performed using ChromaTOF (V 4.3x, LECO) software. Metabolite identification was carried out using the LECO-Fiehn Rtx5 database by matching the mass spectrum and retention index.

### 2.11. Untargeted fecal metabolomics using a high-performance liquid chromatography-MS (HPLC-MS)

Fecal samples were extracted in methanol/acetonitrile (ACN)/$H_2O$ (v:v:v = 2:2:1). To precipitate proteins, samples were mixed and incubated at −20 °C for 1 h. Supernatants were obtained by centrifuging at 12 000$g$ for 15 min at 4 °C. Quality control samples consisted of aliquots of mixed supernatants.

Samples were analyzed using an ultra-high-performance liquid chromatography (UHPLC) system (Vanquish, Thermo Fisher Scientific, USA) with a Phenomenex Kinetex C18 column (2.1 mm × 100 mm, 2.6 μm) coupled to an Orbitrap Exploris 120 mass spectrometer (Orbitrap MS, Thermo Fisher Scientific). Mobile phases A and B were 0.01% aqueous acetic acid and isopropanol: acetonitrile (1:1, v/v), respectively. The autosampler temperature was 4 °C. MS data were acquired in information-dependent acquisition mode. The electrospray ionization source sheath gas flow rate was 50 atmospheres, capillary temperature was 320 °C, MS resolution was 60 000, MS/MS resolution was 15 000, collision energies were stepped normalized collision energy 20/30/40, and spray voltage was 3.8 kV (positive) or −3.4 kV (negative) [32].

R was used to process the data, which were converted to mzXML format for peak detection, extraction, alignment, and integration. The MS2 database (BiotreeDB, China) was used for metabolite annotation, with a cutoff for annotation set at 0.3.

### 2.12. Untargeted serum metabolomics using an HPLC-MS

Methanol with an internal standard was used to extract serum samples (v:v = 4:1). The mixtures were centrifuged at 12 000$g$ for 10 min at 4 °C, after which the supernatants were vacuum freeze-dried (Labconco, USA). UPLC (LC-40D X3, Shimadzu, Japan) and quadrupole TOF-MS systems (TripleTOF 7600, AB SCIEX, USA) were used for untargeted analysis.

Bridged ethyl hybrid (BEH) C8 (2.1 mm × 100 mm, 1.7 μm) UPLC columns (Milford, USA) and C8 guard columns (2.1 mm × 10 mm, 1.7 μm) were used in positive ion mode for detection, with 0.1% aqueous formic acid and 0.1% ACN/formic acid as mobile phases A and B, respectively. High strength silica (HSS) T3 (2.1 mm × 100 mm, 1.8 μm) UPLC columns (Milford) and T3 guard columns (2.1 mm × 10 mm, 1.8 μm) were used in negative ion mode for detection. We used 6.5 mmol·L$^{-1}$ $NH_4HCO_3$ in water and 6.5 mmol·L$^{-1}$ $NH_4HCO_3$ in methanol/water (95/5, v/v) as mobile phases A and B, respectively [33].

### 2.13. Targeted metabolomics using an HPLC-MS

Methanol/water (4:1, v/v) was used to extract metabolites from feces, skin tissues, and serum samples. The suspensions were centrifuged at 12 000$g$ for 10 min at 4 °C, and the supernatants were aspirated and dried in a vacuum dryer.

Trp and indole-3-lactic acid (ILA) were detected using a UHPLC system (LC-40D X3, Shimadzu) coupled to a quadrupole-TOF-MS (TripleTOF 7600, AB SCIEX). BEH C18 (2.1 mm × 100 mm, 1.7 μm) UPLC columns and C18 guard columns (2.1 mm × 10 mm, 1.7 μm) were used for detection. We used 20 mmol·L$^{-1}$ ammonium acetate and 20 mmol·L$^{-1}$ ammonium acetate in ACN/water (85:15, v/v) as mobile phases A and B, respectively.

Multiple reaction monitoring mode was used to obtain data. The TOF-MS scan mass range was 60–1000 Da, and the accumulation time was 100 ms. For Trp and ILA, product ion scan parameters were as follows: Precursor ions were 205.0972 and 206.0812, respectively; fragment ions were 146.0606 and 117.9000, respectively; declustering potential was 45 V, collision energy was 25 or 40 V, respectively; and Zeno pulsing was on. All data acquisition and analyses were conducted using SCIEX OS (AB SCIEX).

### 2.14. Trp and ILA intervention studies

To investigate the effects of Trp (Macklin, 153-94-6, China) and ILA (Allardin, 1821-52-9, China) on impaired skin barrier function induced by aging, 12-month-old C57BL/6J male mice were divided into six groups ($n$ = 6 per group): control, *Lactobacillus murinus* (Lac, BNCC, ATCC 35020, China), Trp, ILA, Trp and antibiotics (Trp + A), and ILA and antibiotics (ILA + A). The studies were approved by the Animal Experimentation Ethics Committee of the Pony Testing International Group Co., Ltd. (ethics approval code: PONY-2023-FL-18).

### 2.15. AhR antagonist (CH223191) studies

C57BL/6J 12 months old, were randomly divided into five groups ($n$ = 6 per group): ① control, ② Trp, ③ ILA, ④ Trp and CH223191 (Trp + C), and ⑤ ILA and CH223191 (ILA + C). A 10 μmol·L$^{-1}$ solution of CH223191 (301326-22-7, Sigma, USA) was applied to the dorsal skin for 30 minutes before Trp or ILA treatments [34].

### 2.16. Statistical analysis

GraphPad Prism (Version 8; GraphPad Prism Institute, Inc., San Diego, CA, USA) and SPSS 20 software (SPSS Inc., USA) were used to analyze the data. One-way analysis of variance (ANOVA) was used to test for differences between mean values. Tukey's test was used for *post-hoc* analysis following one-way ANOVA. A $p$-value of < 0.05 was considered statistically significant.

## 3. Results

### 3.1. Skin phenotype alterations after FMT

To investigate whether gut microbiota from young mice ameliorated skin aging in aged mice, we evaluated skin phenotypes after FMT (Fig. 1(a)). Water retention significantly increased in Old-Y mice compared to Old mice, as evidenced by skin content assessments (30.8% ± 2.79% in Old-Y mice vs 24.3% ± 1.51% in Old mice; Fig. 1(b)), TEWL measurements ((6.120 ± 0.580) $g{\cdot}m^{-2}{\cdot}h^{-1}$ in Old-Y mice and (12.400 ± 0.840) $g{\cdot}m^{-2}{\cdot}h^{-1}$ in Old mice; Fig. 1(c)), and increased epidermis thickness and collagen volume ratios (11.8 ± 1.03 and 55.1 ± 2.34 in Old-Y mice vs 8.88 ± 1.12 and 45.5 ± 4.96 in Old mice, respectively; Figs. 1(d)–(f)).

Immunofluorescence (IF) analysis of differentiation markers showed a significant increase in cytokeratin-10 expression in the skin of Old-Y mice. In Old mice, tight junction integrity in the skin epithelium was compromised, as evidenced by downregulated and diffuse desmoglein-1 expression in the epidermis (Figs. 1(g) and (h)). Consistent with the collagen volume ratio data (Fig. 1(f)), Western blot results showed significant increases in collagens I and III content in the skin of Old-Y mice compared to Old mice after FMT (Figs. 1(i) and (j)). Additionally, tight junction protein expression (zonula occludens-1 (ZO1), occludin, and claudin-1) in Old-Y mice increased after FMT compared to Old mice (Figs. 1(k)–(m)). Thus, FMT reversed skin aging in aged mice, primarily reflected by increased water content, decreased transcutaneous water loss, increased collagen content, increased thickness, and enhanced differentiation.

### 3.2. Gut microbiota changes after FMT

An antibiotic-treated mouse model was used for FMT to verify the effects of microbiota on aged mice skin. Feces were transplanted from young mice into aged (Old-Y) germ-free mice. Next, α- and β-diversity indices and microbiota composition before and after FMT were compared. After FMT, α-diversity changed, and the diversity indices (Shannon and Chao) moved closer to those of donor mice, with Old-Y showing a significant decrease ($p$ < 0.05; Figs. 2(a) and (b)) in both the Shannon and Chao indices compared to Old mice. Principal coordinates analysis (PCA) results reflected β-diversity in the gut microbiota. As observed (Fig. 2(c)), Old-Y mice clustered with Young mice after FMT, indicating that β-diversity in Old-Y mice was similar to that of Young mice.

In Old-Y mice, after four weeks of FMT, bacterial flora structures were altered, with higher proportions of *Firmicutes* and *Bacteroidetes*, similar to the microbiota of Young mice (Fig. 2(d)). We were particularly interested in characteristic bacterial alterations in the intestine before and after FMT. In Old mice, the most significantly changed genera were *Lactobacillus*, *Kurthia*, *Aerococcus*, and *Lactococcus*, with *Lactobacillus* and *Lactococcus* being more abundant in younger mice and depleted in older mice (Figs. 2(e) and (f)). *Lactobacillus* and *Lactococcus* abundance was significantly upregulated in Old-Y mice after FMT from young mice (Figs. 2(g) and (h)). Additionally, *Candidatus stoquefichus* and *Aerococcus* were simultaneously increased in both Young and Old-Y mice.

### 3.3. Fecal metabolite changes after FMT

The gut microbiota generally affects host health through metabolite expression; therefore, we performed LC-MS and gas chromatography (GC)-MS analyses on mouse feces and detected and identified 2506 metabolites. PCA showed separation among the three groups (Fig. 3(a)) with 23.2%, 19.5% of variation explained by the principal components PC1 and PC2, respectively (analysis of similarities (ANOSIM), $p$ = 0.002, $R^2$ = 0.412). Projection latent structure discriminant analysis (PLS-DA) indicated that the three clusters were significantly separated. Permutation plot tests for the PLS-DA model yielded $R^2X$ (cum) = 0.848, $R^2Y$ (cum) = 0.991, and fitness $Q^2Y$ (cum) = 0.841, which suggested good model reliability and predictability (Figs. 3(b) and (c)).

In volcano plots, $p$-values and multiplicity of differences for all metabolites were estimated. Red and blue points represented significantly upregulated and downregulated metabolites, respectively. We identified 194 and 272 significantly increased and decreased metabolites, respectively, in Old-Y mice compared to Old mice (Figs. 3(d)–(f)). Additionally, 53 and 93 metabolites were significantly upregulated and downregulated, respectively, in Young mice compared to Old mice. Old-Y mice had 267 and 223 significantly upregulated and downregulated metabolites, respectively, compared to Young mice. To determine the most altered metabolites in Old-Y mice, we screened 40metabolites based on $p$-values. ILA ($p = 4.65 \times 10^{-6}$) and $L$-Trp ($p = 1.43 \times 10^{-5}$) were significantly increased in Old-Y mice compared to Old mice (Fig. 3(g)). Furthermore, Kyoto Encyclopedia of Genes and Genomes (KEGG) results showed that the Trp metabolic pathway was significantly enriched in Old-Y mice compared to Old mice (Figs. 3(h) and (i)).

### 3.4. Serum metabolite changes after FMT

To further explore why FMT appeared to rejuvenate skin, we analyzed serum metabolites using untargeted LC-MS assays. A total of 2459 metabolites were detected and identified in serum. Our PCA and PLS-DA results showed that all three serum metabolite group clusters were significantly separated (Figs. 4(a) and (b)). Permutation plot tests for the PLS-DA model for Old-Y and Old mice are shown (Fig. 4(c)) and indicate good model reliability and predictability. Volcano plots of different metabolites between the two groups (Figs. 4(d)–(f)) showed that compared to Old mice, 201 and 423 metabolites were significantly upregulated and downregulated, respectively, in Old-Y mice, while 122 and 201 metabolites were significantly increased and decreased, respectively, in Young mice. Compared to the Young group, 353 metabolites were upregulated and 112 metabolites were downregulated in the Old-Y group. To determine significantly altered metabolites after FMT, we screened for metabolites that were significantly increased in both Old-Y feces and serum. Notably, only Trp and ILA were simultaneously elevated (Figs. 4(g)–(j)). Next, we performed Spearman's correlation analyses of significantly increased bacterial levels in feces and differential metabolites in feces and serum. A significant positive correlation was identified between Trp and ILA and *Lactobacillus* in both feces (Figs. 4(k) and (l)) and serum (Figs. 4(m) and (n)).

### 3.5. Targeted Trp and ILA detection in feces, serum, and skin tissues

Previously, using untargeted metabolomics, we screened for metabolites (Trp and ILA) that were significantly increased after FMT and quantified these metabolites in feces, serum, and skin tissues using targeted metabolomics. Sample processing and LC-MS quantitative analyses are outlined (Fig. S1(a) in Appendix A). The standard curves for Trp ($y$ = 329 386$x$ + 7 128, $R^2$ = 1) and ILA standard curves ($y$ = 82 140$x$ + 454, $R^2$ = 1) are also shown (Figs. S1(b)

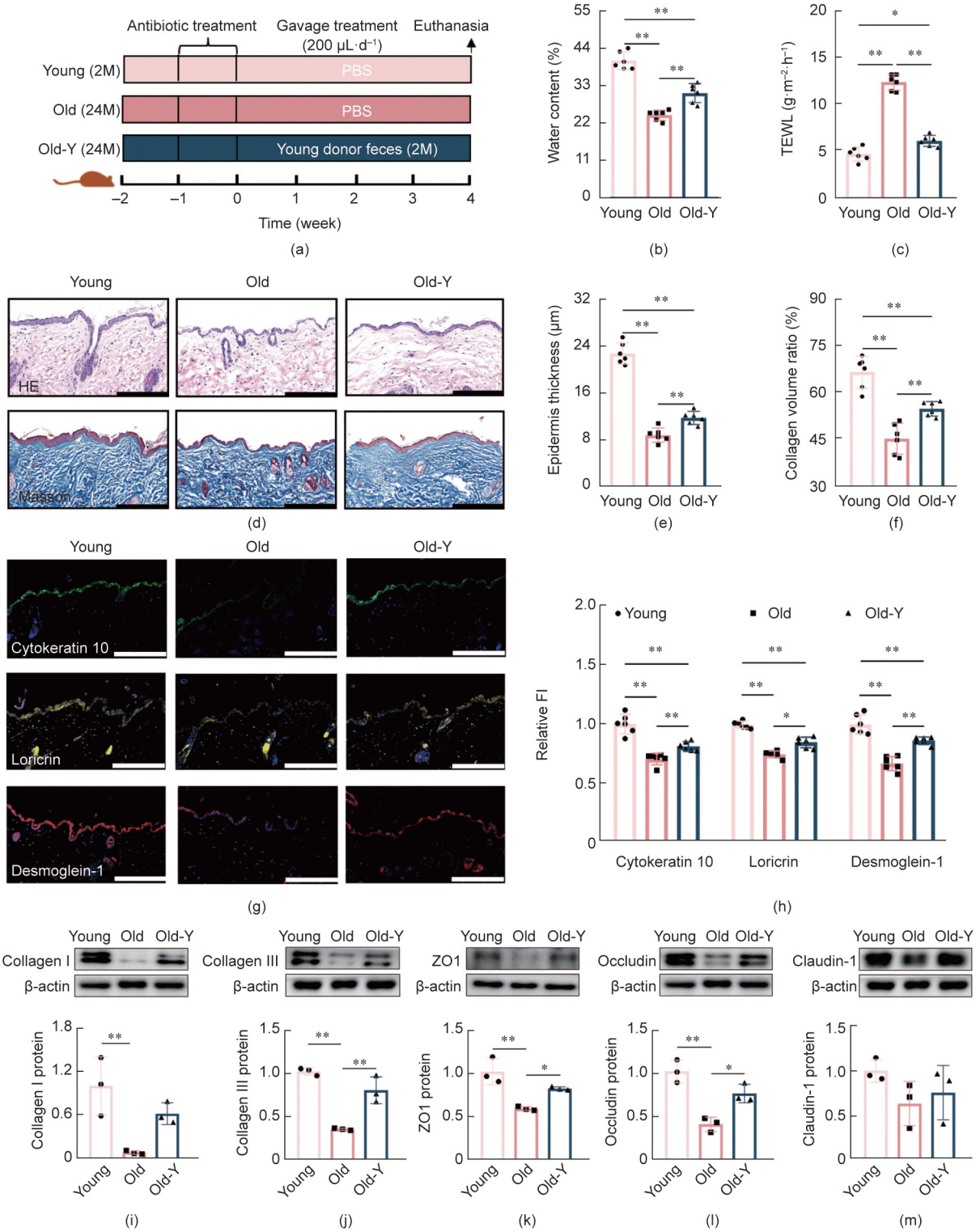


**Fig. 1.** Fecal microbiota transplantation from young into aged mice improves skin barrier function. (a) Schematic showing the study design (M: month). (b) Skin water content in groups ($n$ = 6). (c) Trans-epidermal water loss in groups ($n$ = 6). (d) HE and Masson stained images of skin in different groups. Scale bar = 100 μm. (e) Epidermal thickness results ($n$ = 6). (f) Collagen volume ratios ($n$ = 6). (g) Immunohistochemical cytokeratin 10 (green), loricrin (yellow), and desmoglein-1 (red) staining. Scale bar = 100 μm. (h) Fluorescence intensity (FI) quantification of differentiated proteins ($n$ = 6). (i–m) Representative Western blots (collagen I, collagen III, ZO1, occludin, and claudin-1) ($n$ = 3). One-way ANOVA. *$p$ < 0.05 and **$p$ < 0.01.

and (c) in Appendix A, respectively). As indicated in Figs. S1(d) and (f) in Appendix A, Trp concentrations in feces, serum, and skin tissues were significantly higher in Old-Y mice compared with Old mice ($p$ < 0.05). Furthermore, no significant differences in feces and serum metabolite levels were observed between Young and Old mice, except in skin tissues. As shown in Figs. S1(g)–(i) in Appendix A, ILA concentrations in feces, serum, and skin tissues were significantly higher in Old-Y mice compared with Old mice ($p$ < 0.05), which were consistent with previous trends (Figs. 4 (g)–(j)).

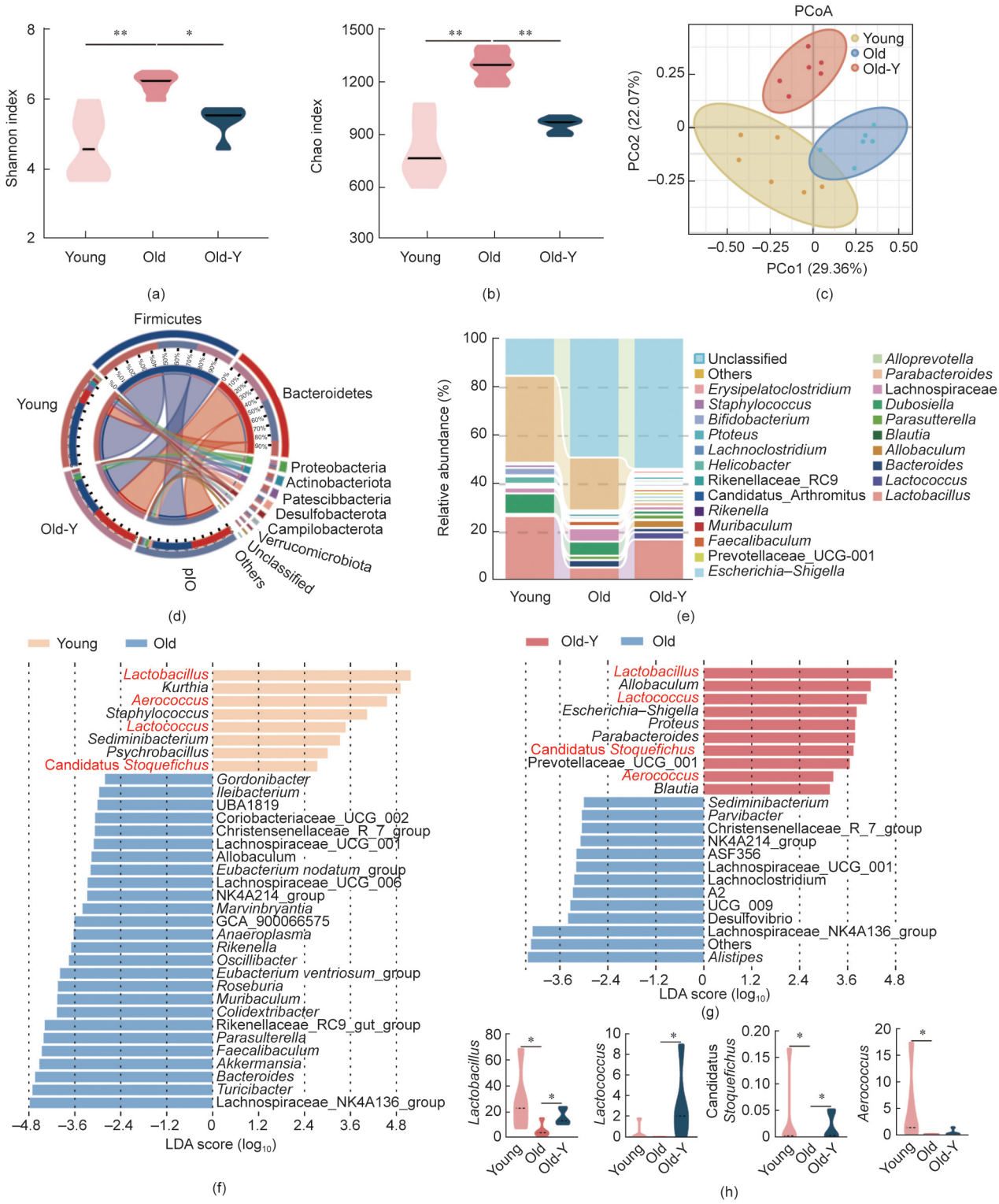


**Fig. 2.** Fecal microbiota composition in fecal microbiota transplanted mice. (a, b) α-diversity evaluations of microbial richness and evenness using Shannon and Chao diversity indices ($n$ = 6). (c) Principal coordinates analysis based on Bray–Curtis results ($n$ = 6). (d) Relative gut microbiota abundance at phylum levels in groups. (e) Relative gut microbiota abundance at genus levels in groups. (f, g) Linear discriminant analysis effect size (LEfSe) was used to identify the differentially bacteria. (h) Relative key microbiota abundance based on LEfSe results ($n$ = 6). LDA: linear discriminant analysis.

### *3.6. Trp and ILA treatment effects on skin phenotypes in aging mice*

Using both untargeted and targeted metabolomics, we observed that Trp and ILA metabolites were significantly increased in Old-Y mice after FMT. Therefore, we speculated that these metabolites might be implicated in rejuvenating skin, so we validated their roles in our models (Fig. 5(a)). We first evaluated water content (Fig. 5(b)) and TEWL values (Fig. 5(c)) in the skin. Water content was significantly higher in the Lac, Trp, ILA, and ILA + A groups compared with the control group ($p < 0.01$). No significant differences were recorded between the Trp + A and control groups. TEWL values were significantly lower in the Lac, Trp, ILA, and ILA

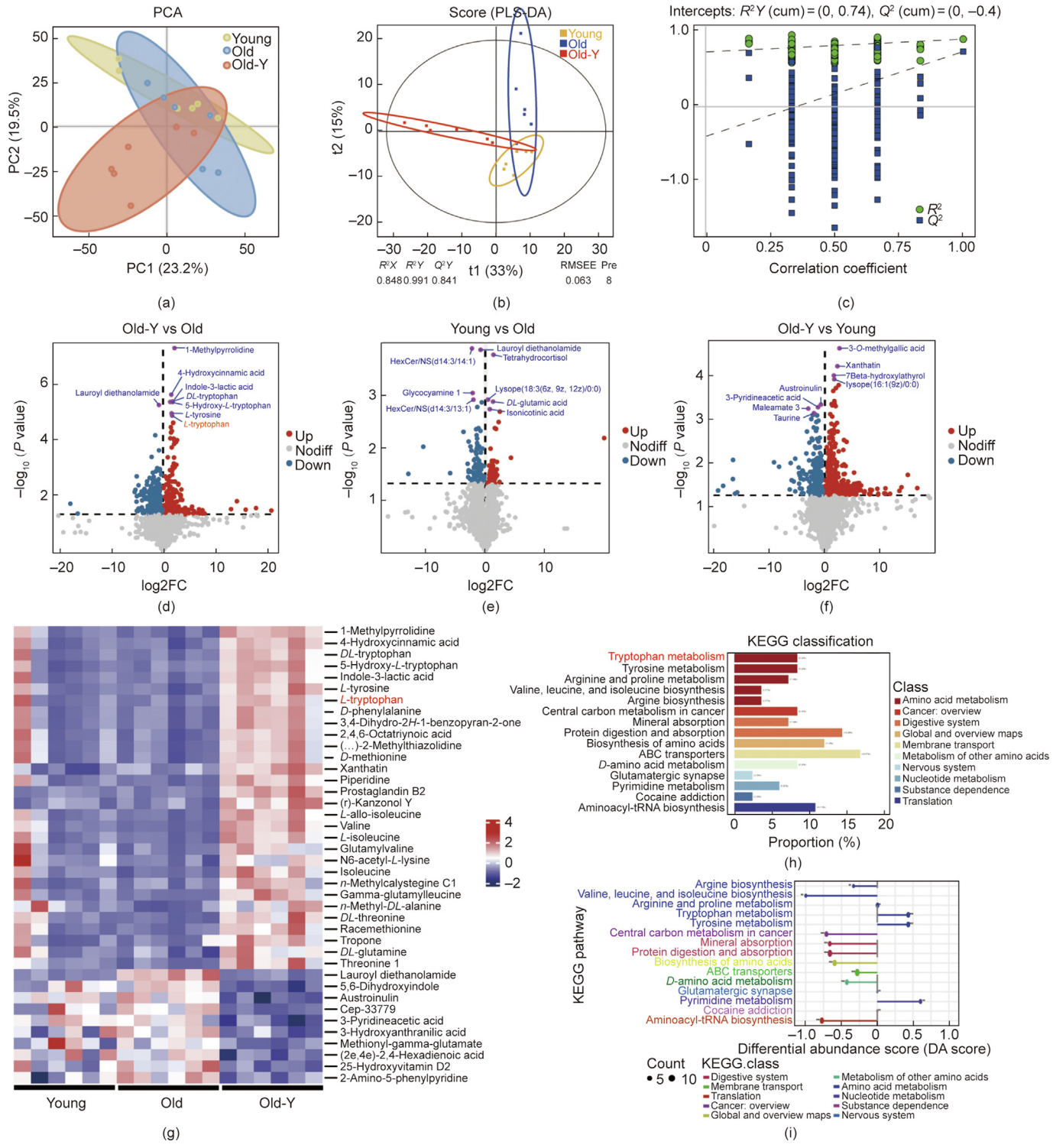


**Fig. 3.** Fecal metabolite composition in fecal microbiota transplanted mice. (a) β-diversity using principal component analysis ($n$ = 6). (b) Projections to latent structures-discriminate analysis score plots on feces ($n$ = 6). (c) Permutation validation plots showing Old-Y and Old mouse groups ($n$ = 6). (d) Volcano plot based on differential metabolite screening between Old-Y and Old mouse groups ($n$ = 6). (e) Volcano plot based on differential metabolite screening between Young and Old mouse groups ($n$ = 6). (f) Volcano plot based on differential metabolite screening between Old-Y and Young mouse groups ($n$ = 6). (g) Relative abundance heatmap showing the relative abundance of key (40) metabolites ($p$ < 0.05, variable important in projection (VIP) > 1). (h) KEGG enrichment pathway map for all fecal metabolites ($n$ = 6). (i) Differential abundance scores for all fecal metabolites ($n$ = 6).

+ A groups compared with the control group ($p$ < 0.01). No significant differences were recorded between the Trp + A and control groups. As shown in Figs. 5(d) and (e), epidermal thickness and collagen volume ratios increased in the Lac, Trp, ILA, and ILA + A groups compared with the control group.

IF results (Figs. 5(f)–(h)) showed that *Lactobacillus*, Trp, and ILA supplementation significantly increased cytokeratin 10, loricrin, and desmoglein-1 protein expression levels in the epidermis compared with the control group ($p$ < 0.01). The effects of *Lactobacillus*, Trp, ILA, and ILA + A supplementation were superior to those of Trp

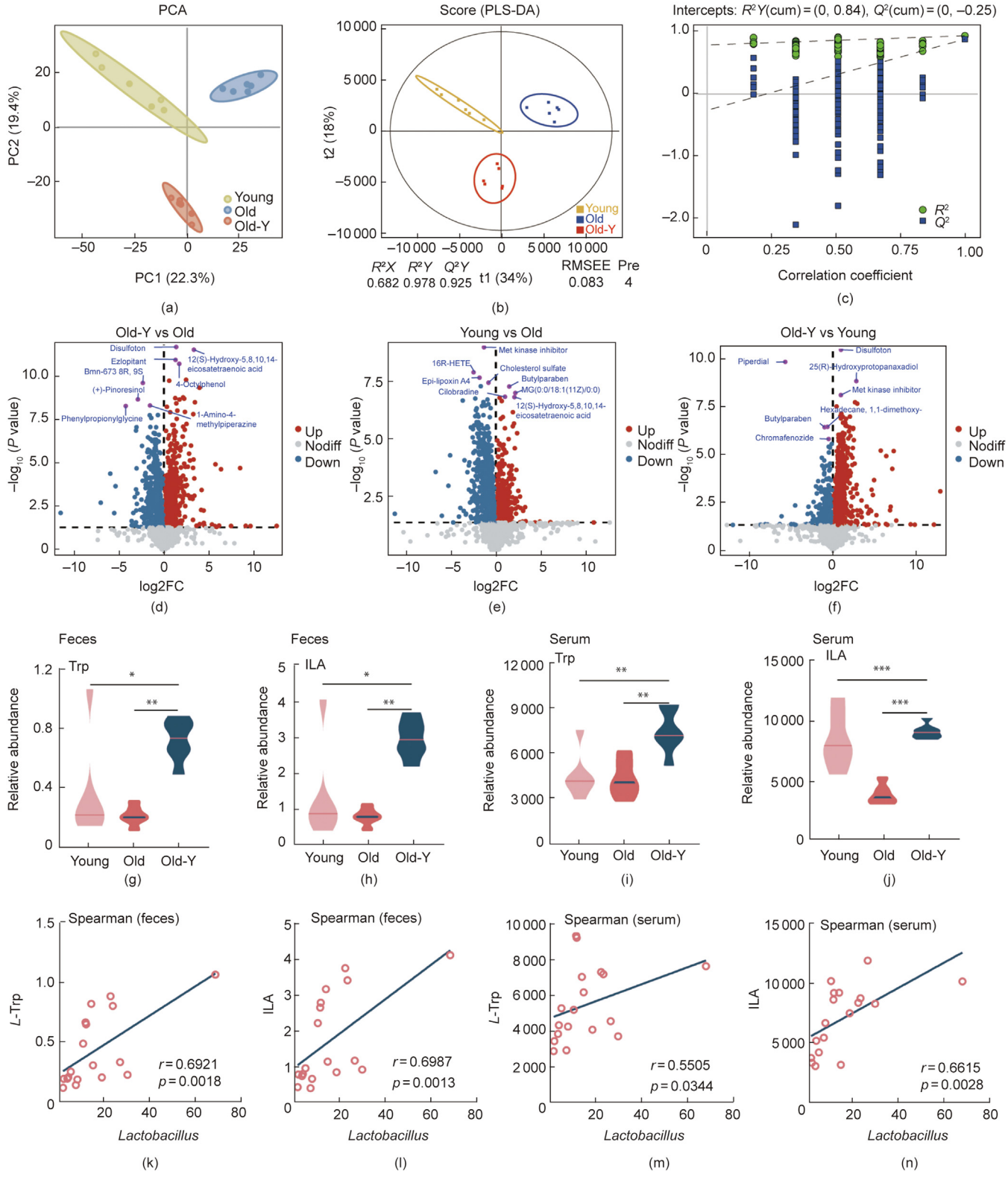


**Fig. 4.** Serum metabolite composition in fecal microbiota transplanted mice. (a) β-diversity using principal component analysis ($n$ = 6). (b) Projections to latent structures-discriminate analysis of score plots on serum ($n$ = 6). (c) Permutation validation plots showing Old-Y and Old mouse groups ($n$ = 6). (d) Volcano plot based on differential metabolite screening between Old-Y and Old mouse groups ($n$ = 6). (e) Volcano plot based on differential metabolite screening between Young and Old mouse groups ($n$ = 6). (f) Volcano plot based on differential metabolite screening between Old-Y and Young mouse groups ($n$ = 6). (g–j) Relative metabolite abundance showing simultaneous increases in feces and serum ($n$ = 6). (k, l) Spearman's correlation analysis between Trp and ILA in feces and *Lactobacillus* ($n$ = 6). (m, n) Spearman's correlation analysis between Trp and ILA in serum and *Lactobacillus* ($n$ = 6). $^{*}p < 0.05$, $^{**}p < 0.01$, $^{***}p < 0.001$.

and antibiotics. As shown in Fig. 5(i), AhR and CYP1A1 expression was significantly increased in the skin of the Lac, Trp, ILA, and ILA + A groups compared with the control group, while no significant changes were recorded in the Trp + A group. Consistent with previous results (Fig. 5(e)), Western blots showed increased collagens I and III content in the skin of the Lac, Trp, ILA, and ILA + A groups

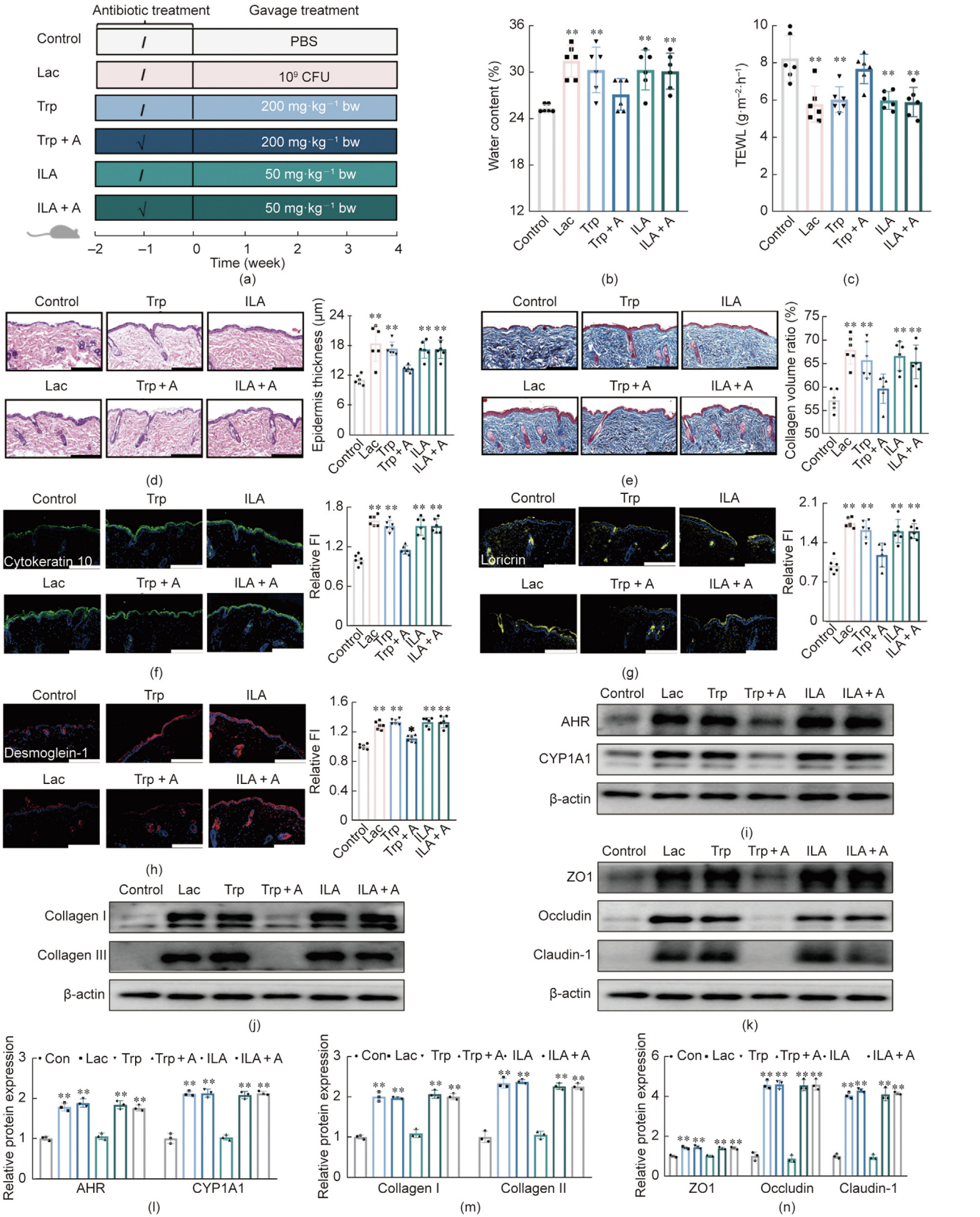


**Fig. 5.** A *Lactobacillus*, Trp, and ILA intervention reverses skin barrier function in aged mice. (a) Schematic showing the study design. bw: body weight. (b) Skin water content in groups ($n$ = 6). (c) TEWL in groups ($n$ = 6). (d) HE images and results showing epidermal thickness in mice. Scale bar = 100 μm ($n$ = 6). (e) Masson staining images of skin and results showing collagen volume ratios. Scale bar = 100 μm ($n$ = 6). (f) Immunohistochemical cytokeratin 10 (green) staining and FI quantification. Scale bar = 100 μm ($n$ = 6). (g) Immunohistochemical loricrin (yellow) staining and FI quantification. Scale bar = 100 μm ($n$ = 6). (h) Immunohistochemical desmoglein-1 (red) staining and FI quantification. Scale bar = 100 μm ($n$ = 6). (i–k) Representative Western blots showing AHR, CYP1A1, collagen I, collagen III, ZO1, occludin, and claudin-1 expression. (l–n) Relative protein expression results ($n$ = 3).

compared with the control group (Fig. 5(j)). Additionally, tight junction protein expression (ZO1, occludin, and claudin-1) in the Lac, Trp, ILA, and ILA + A groups was increased compared with the control group (Fig. 5(k)). Thus, *Lactobacillus*, Trp, and ILA supplementation reversed skin aging in aged mice, which was mainly reflected by increased water content, decreased transcutaneous water loss, increased collagen content, increased skin thickness, and enhanced epidermal differentiation.

### 3.7. Trp and ILA skin aging mechanisms in mice

We observed that Trp and ILA upregulated AhR expression (Fig. 5(i)); therefore, we speculated that these metabolites exert their anti-aging effects via AhR. To examine this hypothesis, we treated mice with CH223191 (an AhR antagonist) and gavaged them with Trp and ILA simultaneously. The experimental design is shown in Fig. 6(a). We first examined water content and TEWL values in the skin and found that Trp and ILA alone significantly increased water content and decreased TEWL values. However, when combined with CH223191, no significant differences in these values were observed compared with the control group (Figs. 6(b) and (c)). Similarly, after simultaneous gavage of Trp, ILA, and CH223191, no significant changes in skin thickness or collagen volume ratios were identified compared with the control group (Figs. 6(d)–(f)). Additionally, no significant differences in AhR and CYP1A1 expression, collagens I and III content, and tight junction protein expression (ZO1, occludin, and claudin-1) were observed in the Trp + C and ILA + C groups. Thus, Trp and ILA did not reverse skin aging when combined with the AhR antagonist CH223191, suggesting that these metabolites exert their anti-aging effects via AhR activation to promote skin epidermal differentiation.

## 4. Discussion

As the largest organ in the body, the skin has not only important physiological functions but also significant social and aesthetic roles. However, with aging, the skin undergoes a decline characterized by decreased water content, collagen content, and epidermal thickness, eventually leading to wrinkling [35]. Thus, reversing skin aging has become a major research focus. During skin aging, the gut microbiota is also disrupted. We hypothesized that the gut microbiota from young mice could improve skin aging in aged mice. Our analyses confirmed that skin aging in aged mice was indeed reversed via FMT from young mice, with Trp and ILA metabolites functioning through AhR activation to promote skin epidermal differentiation.

First, we used an antibiotic-treated mouse model [36]. Fecal bacteria from young mice were transplanted into Old-Y mice, leading to the colonization of Old-Y mice with bacterial flora from young mice. We observed increases in skin water content, epidermal thickness, collagen content, and the expression of differentiated and tight junction proteins (ZO1, occludin, and claudin-1) in Old-Y mice, suggesting that the microbiota from young mice positively influenced skin barrier function [37]. A previous study reported similar findings, where FMT from young to aged mice improved skin aging and overall fitness in aged animals, consistent with our results [30]. Collectively, these data suggest that the microbiota from young mice can reverse skin barrier damage caused by aging.

Data from several studies have shown that skin health is influenced by gut microbes, often referred to as the gut–skin axis [20]. We observed that FMT delayed skin aging in aged mice by reestablishing normal gut flora. Overall, our α- and β-diversity results indicated that the microbiota in Old-Y and young mouse groups were similar. The flora structure and composition in older mice changed after FMT, mainly due to the colonization of beneficial bacteria from younger mice, such as *Lactobacillus* and *Lactococcus*. This suggests that FMT from young mice restored a healthy microbiota in aged mice. *Lactobacillus*, a probiotic, exerts many beneficial effects on the body. Several *Lactobacillus* strains have been identified as functional probiotics, providing benefits such as eliminating pathogenic bacteria [38,39], improving the intestinal barrier [40], modulating the immune system [41], exhibiting anticancer activity [42], and delaying skin aging [43]. In their study, Levkovich et al. [44] supplemented mice with *Lactobacillus reuteri* probiotics, which reduced skin pH, increased skin thickness, and induced shinier skin by enhancing sebocyte production. However, there are some limitations to our study. For example, while skin microbiota plays a role in skin function and gut microbiota may influence microbiota in other organs such as the skin [45,46], our study did not examine skin microbiota in aged mice with or without FMT from young mice. Future studies will explore the changes in skin microbiota after FMT from young mice and their effects on skin function.

We hypothesized that these beneficial bacteria might help rejuvenate the skin through metabolite expression, which we examined in feces and serum from FMT-treated mice. We were surprised to find that *L*-Trp and ILA levels were increased in both feces and serum from Old-Y mice. Our KEGG results also indicated that metabolites in the feces of Old-Y mice were primarily related to Trp metabolism compared with Old mice. Additionally, we quantified Trp and ILA concentrations in mouse feces, serum, and skin tissues to corroborate the untargeted metabolome data. Trp is an essential amino acid that cannot be synthesized by the body and must be obtained through dietary sources. As a key precursor in protein biosynthesis, Trp is necessary for maintaining gut barrier integrity and immunity and has been shown to reverse neurodegeneration and skin inflammation in aging mice [47–49].

The intestinal microbiota has been previously shown to influence Trp metabolism; for example, indole and its derivatives are established as intestinal Trp metabolites [50]. The literature also suggests that *Lactobacillus* exerts cancer-inhibiting effects via the Trp metabolite ILA [51]. Therefore, we hypothesized that Trp might be involved in reversing skin aging via ILA. To test this, we conducted Trp/ILA gavage studies to evaluate improvements in aged skin barrier functions. Notably, both Trp and ILA alone significantly reversed skin barrier disruption due to aging. However, simultaneous application of Trp and antibiotics weakened the effects of Trp. In contrast, the simultaneous use of ILA and antibiotics did not alter its efficacy. These results demonstrate that intestinal flora plays a crucial role in the anti-aging function of Trp and that Trp improves skin function through ILA.

Skin barrier functions include mechanical, microbial, chemical, and immune barriers. Mechanical barriers comprise tight junctions, adhesion complexes, the stratum corneum, and the cytoskeleton [52,53]. AhR is expressed in various barrier tissues, including the skin. In keratinocytes, AhR is critical for skin cell differentiation, with AhR receptor-deficient mice exhibiting increased transdermal water loss and impaired skin barriers [28,54]. In our study, we explored the mechanisms through which Trp and ILA exert anti-aging effects. We used the AhR inhibitor CH223191 to block AhR activation and simultaneously administered Trp and ILA to mice to observe changes in skin barrier function. We found that the AhR target gene CYP1A1, previously identified in human skin and keratinocytes, was reduced by CH223191, indicating inhibition of the AhR pathway. Previous studies have shown that AhR-deficient mice exhibit enhanced inflammation in praziquantel-induced psoriasis-like skin inflammation [55]. Similarly, coal tar has been shown to induce epidermal differentiation, restore filaggrin protein expression, and improve skin barrier proteins in an AhR-dependent manner by activating AhR [56]. Other studies also demonstrated that *Lactobacillus* metabolizes Trp to produce AhR ligands such as indole-3-formaldehyde, which stimulates interleukin-22 production [57].

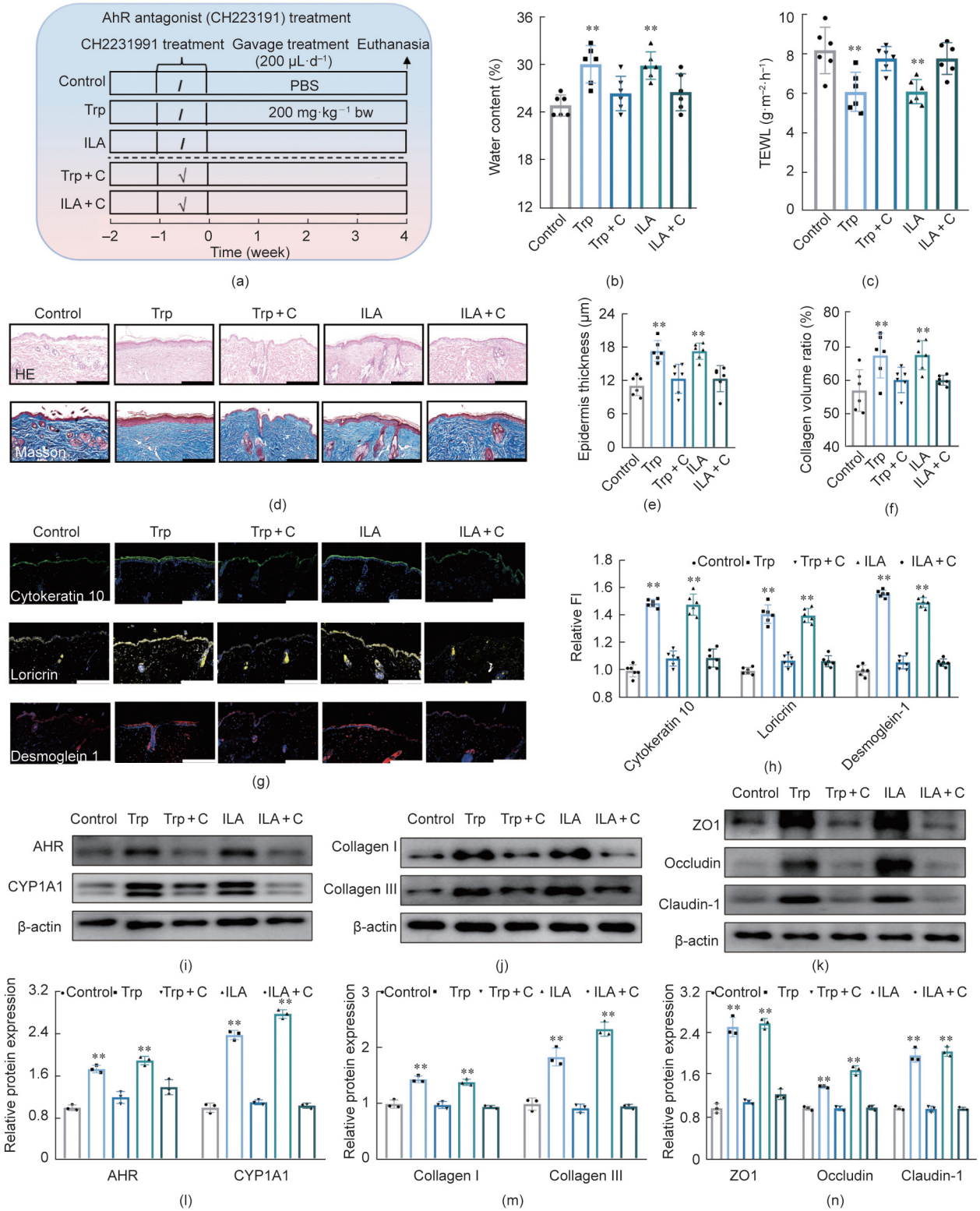


**Fig. 6.** The effects of a simultaneous intervention with the CH223191 antagonist and Trp/ILA in aged mice. (a) Schematic showing the study design. (b) Skin content in groups ($n$ = 6). (c) TEWL in groups ($n$ = 6). (d) HE and Masson staining images showing the skin in different groups. Scale bar = 100 μm. (e) Epidermal thickness results in mice ($n$ = 6). (f) Collagen volume ratio results ($n$ = 6). (g) Immunohistochemical cytokeratin10 (green), loricin (yellow), and desmoglein-1 (red) staining. Scale bar = 100 μm. (h) FI quantification ($n$ = 6). (i–k) Representative Western blots showing AHR, CYP1A1, collagen I, collagen III, ZO1, occludin, and claudin-1 expression. (l–n) Relative protein expression results ($n$ = 3). One-way ANOVA analysis of variance. ** $p < 0.01$.

## 5. Conclusions

In conclusion, our results demonstrated that skin aging can be alleviated by fecal microbiota transplantation (FMT) from young mice to aged mice. Trp and ILA metabolites, produced by probiotics such as *Lactobacillus* and *Lactococcus*, trigger communication between the gut and the skin. Thus, replenishing *Lactobacillus*, Trp, and ILA can achieve similar effects to FMT. Both Trp and ILA

improve skin epidermal differentiation via the AhR pathway. Therefore, supplementation with probiotics or their metabolic products may be a potential strategy for improving skin aging.

## Acknowledgment

This project was supported in part by grants from the National Key Research and Development Program of China (2021YFD1600204 and 2023YFF1104500) and the 111 project from the Ministry of Education of the People's Republic of China 577 (B18053).

## Compliance with ethics guidelines

Shoujuan Yu, Ziyang Li, Xiaoxu Zhang, Qi Zhang, Liwei Zhang, Liang Zhao, Ping Liu, Jie Guo, Juan Chen, Chengying Zhang, Xinjuan Liu, Mengyang Yu, Dekui Jin, Xiaofeng Wang, Guang Li, Yan Cao, Fazheng Ren, and Ran Wang declare that they have no conflicts of interest or financial conflicts to disclose.

## Appendix A. Supplementary data

Supplementary data to this article can be found online at https://doi.org/10.1016/j.eng.2024.08.005.

## References

[1] Waller JM, Maibach HI. Age and skin structure and function, a quantitative approach (I): blood flow, pH, thickness, and ultrasound echogenicity. Skin Res Technol 2005;11(4):221–35.
[2] López-Otín C, Blasco MA, Partridge L, Serrano M, Kroemer G. The hallmarks of aging. Cell 2013;153(6):1194–217.
[3] McLean AJ, Le Couteur DG. Aging biology and geriatric clinical pharmacology. Pharmacol Rev 2004;56(2):163–84.
[4] Gracia-Cazaña T, González S, Parrado C, Juarranz Á, Gilaberte Y. Influence of the exposome on skin cancer. Actas Dermosifiliogr 2020;111(6):460–70.
[5] Liu N, Matsumura H, Kato T, Ichinose S, Takada A, Namiki T, et al. Stem cell competition orchestrates skin homeostasis and ageing. Nature 2019;568(7752):344–50.
[6] Koester J, Miroshnikova YA, Ghatak S, Chacón-Martínez CA, Morgner J, Li X, et al. Niche stiffening compromises hair follicle stem cell potential during ageing by reducing bivalent promoter accessibility. Nat Cell Biol 2021;23(7):771–81.
[7] Mahmoudi S, Mancini E, Xu L, Moore A, Jahanbani F, Hebestreit K, et al. Heterogeneity in old fibroblasts is linked to variability in reprogramming and wound healing. Nature 2019;574(7779):553–8.
[8] Giangreco A, Qin M, Pintar JE, Watt FM. Epidermal stem cells are retained *in vivo* throughout skin aging. Aging Cell 2008;7(2):250–9.
[9] Doles J, Storer M, Cozzuto L, Roma G, Keyes WM. Age-associated inflammation inhibits epidermal stem cell function. Genes Dev 2012;26(19):2144–53.
[10] Benitah SA, Welz PS. Circadian regulation of adult stem cell homeostasis and aging. Cell Stem Cell 2020;26(6):817–31.
[11] Choi EH. Aging of the skin barrier. Clin Dermatol 2019;37(4):336–45.
[12] Zhang HL, Sun H, Yang YF, Li YM. Skin substitutes comprised of recombinant human collagen hydrogel promote full-thickness skin defect reconstruction. Burns 2022;48(6):1523–4.
[13] Truswell WH. Prescription skin care products and skin rejuvenation. Facial Plast Surg Clin North Am 2020;28(1):59–65.
[14] Murad H, Tabibian MP. The effect of an oral supplement containing glucosamine, amino acids, minerals, and antioxidants on cutaneous aging: a preliminary study. J Dermatolog Treat 2001;12(1):47–51.
[15] Zhang S, Duan E. Fighting against skin aging: the way from bench to bedside. Cell Transplant 2018;27(5):729–38.
[16] Jwo JY, Chang YT, Huang YC. Effects of probiotics supplementation on skin photoaging and skin barrier function: a systematic review and meta-analysis. Photodermatol Photoimmunol Photomed 2023;39(2):122–31.
[17] De Pessemier B, Grine L, Debaere M, Maes A, Paetzold B, Callewaert C. Gut–skin axis: current knowledge of the interrelationship between microbial dysbiosis and skin conditions. Microorganisms 2021;9(2):353.
[18] Chen L, Li J, Zhu W, Kuang Y, Liu T, Zhang W, et al. Skin and gut microbiome in psoriasis: gaining insight into the pathophysiology of it and finding novel therapeutic strategies. Front Microbiol 2020;11:589726.
[19] Fang Z, Pan T, Li L, Wang H, Zhu J, Zhang H, et al. Bifidobacterium longum mediated tryptophan metabolism to improve atopic dermatitis via the gut–skin axis. Gut Microbes 2022;14(1):2044723.
[20] Yu Y, Wang W, Zhang F. The next generation fecal microbiota transplantation: to transplant bacteria or virome. Adv Sci 2023;10(35):2301097.
[21] Junca H, Pieper DH, Medina E. The emerging potential of microbiome transplantation on human health interventions. Comput Struct Biotechnol J 2022;20:615–27.
[22] Suskind DL, Brittnacher MJ, Wahbeh G, Shaffer ML, Hayden HS, Qin X, et al. Fecal microbial transplant effect on clinical outcomes and fecal microbiome in active Crohn's disease. Inflamm Bowel Dis 2015;21(3):556–63.
[23] Vongsavath T, Rahmani R, Tun KM, Manne V. The use of fecal microbiota transplant in overcoming and modulating resistance to anti-pd-1 therapy in patients with skin cancer. Cancers 2024;16(3):499.
[24] Jiang X, Liu Z, Ma Y, Miao L, Zhao K, Wang D, et al. Fecal microbiota transplantation affects the recovery of AD-skin lesions and enhances gut microbiota homeostasis. Int Immunopharmacol 2023;118:110005.
[25] Mou Y, Du Y, Zhou L, Yue J, Hu X, Liu Y, et al. Gut microbiota interact with the brain through systemic chronic inflammation: implications on neuroinflammation, neurodegeneration, and aging. Front Immunol 2022;13:796288.
[26] Parker A, Romano S, Ansorge R, Aboelnour A, Le Gall G, Savva GM, et al. Fecal microbiota transfer between young and aged mice reverses hallmarks of the aging gut, eye, and brain. Microbiome 2022;10(1):68.
[27] Shin J, Noh JR, Choe D, Lee N, Song Y, Cho S, et al. Ageing and rejuvenation models reveal changes in key microbial communities associated with healthy ageing. Microbiome 2021;9(1):240.
[28] Boehme M, Guzzetta KE, Bastiaanssen TFS, van de Wouw M, Moloney GM, Gual-Grau A, et al. Microbiota from young mice counteracts selective age-associated behavioral deficits. Nat Aging 2021;1(8):666–76.
[29] Lee J, d'Aigle J, Atadja L, Quaicoe V, Honarpisheh P, Ganesh BP, et al. Gut microbiota-derived short-chain fatty acids promote poststroke recovery in aged mice. Circ Res 2020;127(4):453–65.
[30] Kim KH, Chung Y, Huh JW, Park DJ, Cho Y, Oh Y, et al. Gut microbiota of the young ameliorates physical fitness of the aged in mice. Microbiome 2022;10(1):238.
[31] Wei W, Wong CC, Jia Z, Liu W, Liu C, Ji F, et al. *Parabacteroides distasonis* uses dietary inulin to suppress NASH via its metabolite pentadecanoic acid. Nat Microbiol 2023;8(8):1534–48.
[32] Li Q, Chan H, Liu WX, Liu CA, Zhou Y, Huang D, et al. *Carnobacterium maltaromaticum* boosts intestinal vitamin D production to suppress colorectal cancer in female mice. Cancer Cell 2023;41(8):1450–65.
[33] Shen X, Wang R, Xiong X, Yin Y, Cai Y, Ma Z, et al. Metabolic reaction network-based recursive metabolite annotation for untargeted metabolomics. Nat Commun 2019;10(1):1516.
[34] Yu J, Luo Y, Zhu Z, Zhou Y, Sun L, Gao J, et al. A tryptophan metabolite of the skin microbiota attenuates inflammation in patients with atopic dermatitis through the aryl hydrocarbon receptor. J Allergy Clin Immunol 2019;143(6):2108–19.
[35] Wang T, Qin Y, Qiao J, Liu Y, Wang L, Zhang X. Overexpression of SIRT6 regulates NRF2/HO-1 and NF-κB signaling pathways to alleviate UVA-induced photoaging in skin fibroblasts. J Photochem Photobiol B 2023;249:112801.
[36] Jing Y, Yu Y, Bai F, Wang L, Yang D, Zhang C, et al. Effect of fecal microbiota transplantation on neurological restoration in a spinal cord injury mouse model: involvement of brain-gut axis. Microbiome 2021;9(1):59.
[37] Li W, Wang Z, Cao J, Dong Y, Chen Y. Melatonin improves skin barrier damage caused by sleep restriction through gut microbiota. J Pineal Res 2023;75(1):12874.
[38] Zhang Q, Li G, Zhao W, Wang X, He J, Zhou L, et al. Efficacy of *bifidobacterium animalis* subsp. *lactis* BL-99 in the treatment of functional dyspepsia: a randomized placebo-controlled clinical trial. Nat Commun 2024;15(1):227.
[39] Stones DH, Krachler AM. Against the tide: the role of bacterial adhesion in host colonization. Biochem Soc Trans 2016;44(6):1571–80.
[40] Wang L, Alammar N, Singh R, Nanavati J, Song Y, Chaudhary R, et al. Gut microbial dysbiosis in the irritable bowel syndrome: a systematic review and meta-analysis of case-control studies. J Acad Nutr Diet 2020;120(4):565–86.
[41] Gill H, Prasad J. Probiotics, immunomodulation, and health benefits. Adv Exp Med Biol 2008;606:423–54.
[42] Uccello M, Malaguarnera G, Basile F, D'agata V, Malaguarnera M, Bertino G, et al. Potential role of probiotics on colorectal cancer prevention. BMC Surg 2012;12(Suppl 1):S35.
[43] Liu Y, Chen K, Li F, Gu Z, Liu Q, He L, et al. Probiotic lactobacillus rhamnosus GG prevents liver fibrosis through inhibiting hepatic bile acid synthesis and enhancing bile acid excretion in mice. Hepatology 2020;71(6):2050–66.
[44] Levkovich T, Poutahidis T, Smillie C, Varian BJ, Ibrahim YM, Lakritz JR, et al. Probiotic bacteria induce a 'glow of health'. PLoS One 2013;8(1):53867.
[45] Hashimoto K. Emerging role of the host microbiome in neuropsychiatric disorders: overview and future directions. Mol Psychiatry 2023;28(9):3625–37.
[46] Shinno-Hashimoto H, Hashimoto Y, Wei Y, Chang L, Fujita Y, Ishima T, et al. Abnormal composition of microbiota in the gut and skin of imiquimod-treated mice. Sci Rep 2021;11(1):11265.
[47] Xue C, Li G, Zheng Q, Gu X, Shi Q, Su Y, et al. Tryptophan metabolism in health and disease. Cell Metab 2023;35(8):1304–26.
[48] Yin J, Zhang B, Yu Z, Hu Y, Lv H, Ji X, et al. Ameliorative effect of dietary tryptophan on neurodegeneration and inflammation in *D*-galactose-induced aging mice with the potential mechanism relying on AMPK/SIRT1/PGC-1α pathway and gut microbiota. J Agric Food Chem 2021;69(16):4732–44.
[49] Guenin-Macé L, Morel JD, Doisne JM, Schiavo A, Boulet L, Mayau V, et al. Dysregulation of tryptophan catabolism at the host-skin microbiota interface in hidradenitis suppurativa. JCI Insight 2020;5(20):140598.

[50] Zhang Q, Zhao Q, Li T, Lu L, Wang F, Zhang H, et al. Lactobacillus plantarum-derived indole-3-lactic acid ameliorates colorectal tumorigenesis via epigenetic regulation of CD8$^+$ T cell immunity. Cell Metab 2023;35(6):943–60.
[51] Huang R, Wu F, Zhou Q, Wei W, Yue J, Xiao B, et al. Lactobacillus and intestinal diseases: mechanisms of action and clinical applications. Microbiol Res 2022;260:127019.
[52] Eyerich S, Eyerich K, Traidl-Hoffmann C, Biedermann T. Cutaneous barriers and skin immunity: differentiating a connected network. Trends Immunol 2018;39(4):315–27.
[53] Simpson CL, Patel DM, Green KJ. Deconstructing the skin: cytoarchitectural determinants of epidermal morphogenesis. Nat Rev Mol Cell Biol 2011;12(9):565–80.
[54] Furue M, Hashimoto-Hachiya A, Tsuji G. Aryl hydrocarbon receptor in atopic dermatitis and psoriasis. Int J Mol Sci 2019;20(21):5424.
[55] Di Meglio P, Duarte JH, Ahlfors H, Owens ND, Li Y, Villanova F, et al. Activation of the aryl hydrocarbon receptor dampens the severity of inflammatory skin conditions. Immunity 2014;40(6):989–1001.
[56] Van den Bogaard EH, Bergboer JG, Vonk-Bergers M, van Vlijmen-Willems IM, Hato SV, van der Valk PG, et al. Coal tar induces AHR-dependent skin barrier repair in atopic dermatitis. J Clin Invest 2013;123(2):917–27.
[57] Zelante T, Iannitti RG, Cunha C, De Luca A, Giovannini G, Pieraccini G, et al. Tryptophan catabolites from microbiota engage aryl hydrocarbon receptor and balance mucosal reactivity via interleukin-22. Immunity 2013;39(2):372–85.